JACS
JOURNAL OF THE AMERICAN CHEMICAL SOCIETY
pubs.acs.org/JACS
Article

Bottom-Up Synthesis of Metalated Carbyne Ribbons via Elimination Reactions

Wenze Gao,[§] Liangliang Cai,[§] Faming Kang, Lina Shang, Mali Zhao, Chi Zhang, and Wei Xu*

Cite This: J. Am. Chem. Soc. 2023, 145, 6203−6209

ABSTRACT: Elimination reactions are one of the most important reactions in organic synthesis, especially in the formation of alkenes and alkynes. Herein, based on scanning tunneling microscopy, we report the bottom-up synthesis of one-dimensional carbyne-like nanostructures, metalated carbyne ribbons with the incorporation of Cu or Ag atoms, through α- and β-elimination reactions of tetrabromomethane and hexabromoethane on surfaces. Density functional theory calculations demonstrate a width-dependent band gap modulation within these ribbon structures, which is affected by interchain interactions. Moreover, mechanistic insights into the on-surface elimination reactions have also been provided in this study.

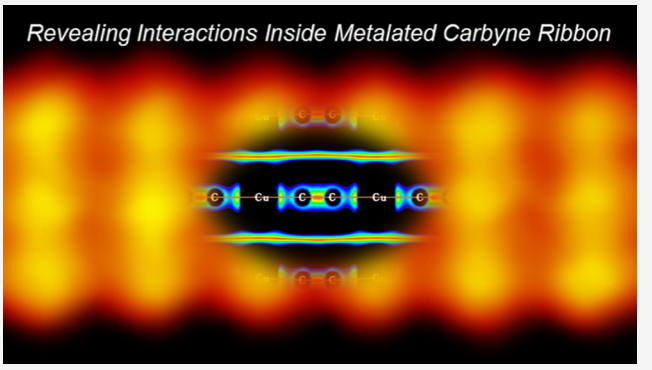

INTRODUCTION

The discovery and creation of low-dimensional carbon allotropes, such as zero-dimensional (0D) fullerenes,[1] one-dimensional (1D) carbon nanotubes (CNTs),[2] and two-dimensional (2D) graphene,[3] have led to innovations in both chemistry and material science. Carbyne, an infinite 1D carbon chain comprising sp-hybridized carbons, has also been fascinating chemists for decades due to its extraordinary properties in expectation. For example, its Young's modulus and anticipated stiffness are greater than most known carbon allotropes, including diamond, graphene, and CNTs.[4] Nevertheless, carbyne has been much less investigated[5,6] compared to other carbon allotropes owing to its strong chemical activity and extreme instability.[7,8] Intriguingly, toward the ultimate pursuit of carbyne, the metalation of such a 1D carbon chain with well-distributed transition metal atoms is also of great potential in regulating electronic and magnetic properties by combining d-electrons of metals and π-electrons of carbons.[9,10]

Elimination reactions, processes that remove two substituents (atoms or groups) from a molecule, play a fundamental role in organic synthesis since Hanhart and Ingold first studied this process in 1927.[11] It has been widely applied in the formation of alkenes[12−14] and alkynes[15,16] via dehalogenation. The two prominent elimination types are the α- and β-elimination (Scheme 1), generating carbenes/nitrenes and alkenes/alkynes, respectively.[17] Despite the contribution of elimination reactions in generating alkenes and alkynes, it remains less explored to apply them to synthesize long 1D carbon-rich nanostructures such as metalated carbyne due to their insolubility and instability in solution.[18]

Scheme 1. Schematic Illustrations of (a) α-Elimination and (b) β-Elimination Reactions[a]

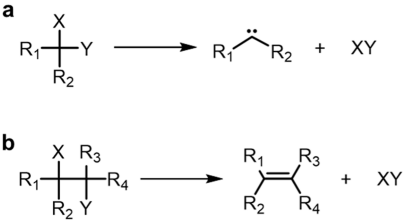

[a]X and Y represent leaving groups.

On-surface synthesis is emerging as a promising approach to fabricating novel sp-carbon nanostructures which are often inaccessible by conventional solution synthesis.[19−22] Metalated carbynes with a series of incorporated metals have been demonstrated to be accessible using a bottom-up approach based on surface-assisted dehydrogenation/dehalogenation and subsequent polymerization, forming isolated chains.[20,22,23] However, the investigation of metalated carbyne chains packing in a metal-to-metal manner (i.e., ribbon structure) remains vacant, while such interchain interactions may have a significant impact on their electronic properties.

Received: November 19, 2022
Published: March 10, 2023

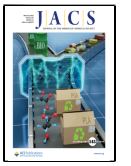

https://doi.org/10.1021/jacs.2c12292
J. Am. Chem. Soc. 2023, 145, 6203−6209

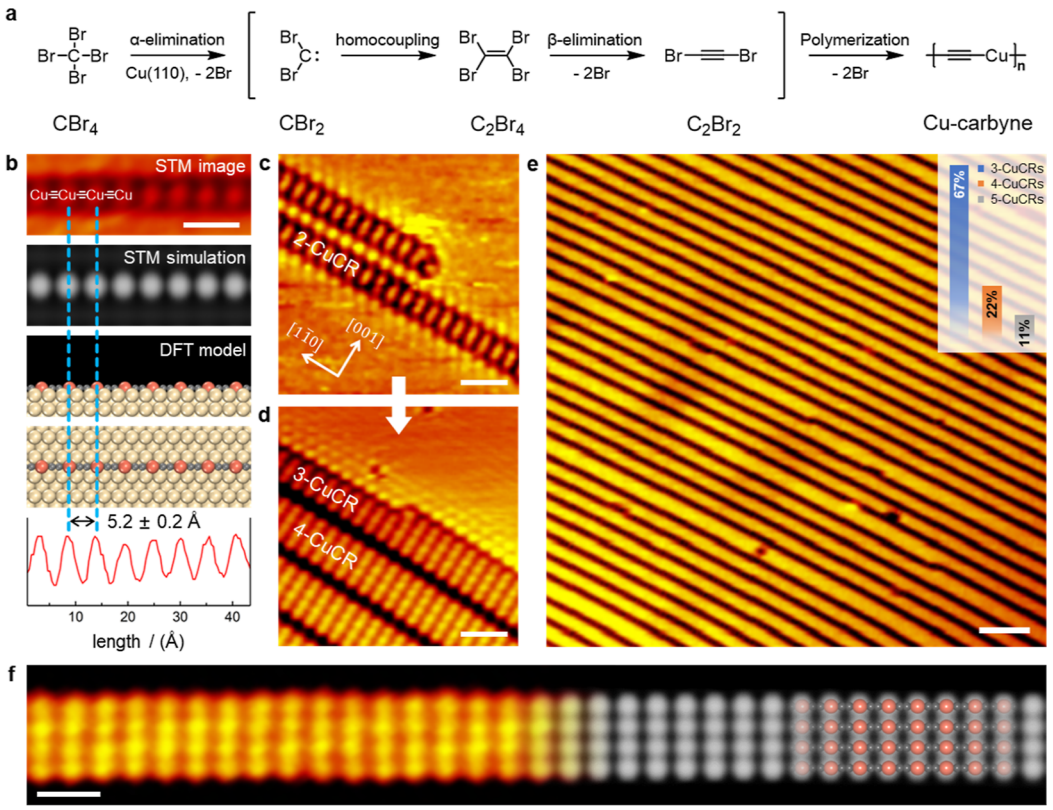

Figure 1. Bottom-up synthesis of CuCRs via α- and β-elimination reactions on Cu(110). (a) Schematic illustration of the bottom-up synthesis of Cu-carbyne via α- and β-elimination reactions. (b) From top to bottom: equally scaled STM image, simulated STM image, side- and top-view of DFT models, and line-scan profile of a single Cu-carbyne chain. Scale bar: 1 nm. (c−e) STM images showing the growth of CuCRs after annealing at (c) 360, (d) 480, and (e) 570 K. Top right panel in (e) histogram depicting the ratio of CuCRs with different widths. Scale bars: (c,d) 1.5 and (e) 5 nm. (f) High-resolution close-up STM image of 4-CuCR (left) combined with a simulated STM image (right), with the corresponding DFT model overlaid. Gray and red balls represent C and Cu atoms, respectively. Scale bar: 1 nm. Typical scanning conditions: V_t = −1767 mV and I_t = 0.66 nA.

In this work, we report a new strategy for the synthesis of metalated carbyne ribbons (MCRs) by using surface-assisted elimination reactions and subsequent polymerization. By the combination of scanning tunneling microscopy (STM) imaging and density functional theory (DFT) calculations, we demonstrated the highly efficient fabrication of Cu-carbyne ribbons (CuCRs) and Ag-carbyne ribbons (AgCRs) from molecular precursors, i.e., tetrabromomethane (CBr_4) and hexabromoethane (C_2Br_6), via α- and β-elimination reactions on Cu(110) and Ag(110), respectively. These MCRs were experimentally visualized in real space, with a characteristic metal-to-metal alignment between adjacent metalated carbynes, which was distinct from the isolated metalated carbynes reported previously.[20,22−24] Moreover, DFT-based transition-state theory calculations demonstrate the elimination reaction processes of both molecular precursors. The interchain interactions and the corresponding density of states (DOS) of the MCRs were further investigated by analysis of wave function, indicating that the face-to-face $\pi-\pi$ stacking between C≡C bonds and the orbital overlap between Cu atoms stabilize the interchain interaction of MCRs. More interestingly, the MCRs exhibit a width-dependent band gap modulation, which could serve as another strategy for engineering the band gap of metalated carbynes compared to the previous study.[24] These results present the availability of elimination reactions in generating new low-dimensional carbyne-like nanostructures, which should enrich the toolbox for the on-surface synthesis of carbon nanostructures and carbon-rich nanomaterials and also contribute to the development of on-surface chemistry.

RESULTS AND DISCUSSION

CBr_4 monomers (as sketched in Figure 1a) were deposited on the clean Cu(110) single-crystal surface held at 300 K by thermal sublimation (with a typical sublimation temperature of 300 K) under ultra-high vacuum conditions, resulting in the formation of isolated 1D chain structures along the close-packed [1$\bar{1}$0] direction of the substrate (Figure 1b). Based on our previous studies,[20,24] these chain structures with a periodicity of 5.2 ± 0.2 Å (Figure 1b) could be naturally attributed to Cu-incorporated metalated carbyne (−Cu−C≡C−), and the protrusions within the chain result from the electronic density of states of Cu atoms. Notably, organometallic species are often formed in dehalogenative coupling reactions.[25,26] Besides, DFT calculations show the correlation between the structural models and simulated STM image, agreeing well with the experimental morphology and periodicity (Figure 1b). The proposed reaction pathway for the formation of Cu-carbyne chains from CBr_4 is illustrated in Figure 1a.

To further understand the reaction pathways of the CBr_4 molecule on Cu(110), DFT calculations were applied to investigate the debromination processes, as demonstrated in Figure 2. As shown in Figure 2b, two Br atoms detached from

https://doi.org/10.1021/jacs.2c12292
J. Am. Chem. Soc. 2023, 145, 6203−6209

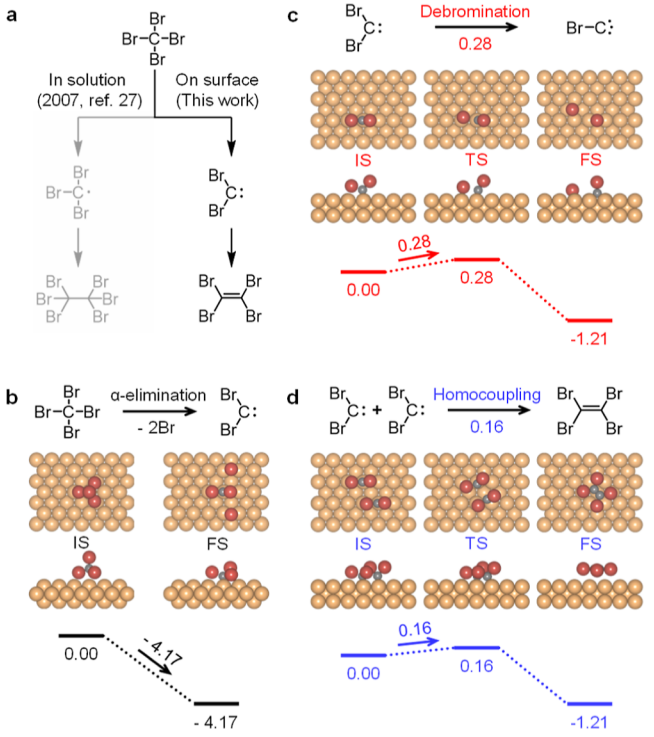

Figure 2. On-surface reaction pathways of the CBr_4 molecule on Cu(110). (a) Schematic illustration showing the difference between the debromination pathways of CBr_4 in solution[27] and on surface. (b) Initial and corresponding DFT-optimized structure of CBr_4 on the Cu(110) surface. Two Br atoms are detached from the C atom spontaneously after DFT optimization. (c,d) DFT-calculated reaction pathways for (c) debromination and (d) homocoupling of CBr_2 intermediate on Cu(110), respectively. The energy scale is not linear. The structural models are given for the initial, transition, and final states, respectively. Gray, red, and light brown balls represent C, Br, and Cu atoms, respectively. Energies are given in units of eV.

the CBr_4 molecule spontaneously on the Cu(110) surface after optimization with no reaction barrier, leaving the CBr_2 group (as a carbene) stabilized by the underlying surface. This can be seen as a typical α-elimination reaction process catalyzed by the Cu(110) substrate, which is different from the debromination pathways of CBr_4 in solution (Figure 2a).[27] For the next step, the competitive reaction pathways of further debromination or homocoupling of CBr_2 intermediates are compared. As shown in Figure 2c,d, the energy barrier of homocoupling (0.16 eV) is lower than debromination (0.28 eV), indicating that the CBr_2 intermediate is very likely to go through the pathway of homocoupling, forming C_2Br_4 intermediate, instead of debromination. In addition, the C_2Br_4 intermediate is also unstable on Cu(110) and easily transforms to C_2Br_2 with the para-Br atom detached spontaneously after the removal of one Br atom (Figure S1), which can be seen as a typical β-elimination reaction process. Finally, C_2Br_2 intermediates further debrominate and polymerize to Cu-carbyne chains, as illustrated in Figure 1a. Thus, based on DFT calculations, we demonstrate that CBr_4 molecules undergo surface-catalyzed α- and β-elimination reaction processes and form Cu-carbyne chains by subsequent debromination and polymerization.

Interestingly, upon annealing the sample to ~360 and 480 K, respectively, Cu-carbyne chains started to assemble together and grow into ribbon structures, as shown in Figure 1c,d. Further annealing to ~570 K resulted in the formation of highly ordered CuCRs along the $[1\bar{1}0]$ direction of Cu(110) with different widths, as can be seen from the large-scale STM image (Figure 1e). The histogram depicted in Figure 1e displays the approximate ratio of different types of *N*-CuCRs (*N* is the number of the Cu-carbyne chains across the ribbon) observed. The comparison between the high-resolution STM image of 4-CuCR and the corresponding STM simulation with the DFT-models overlaid showed that both the dimension and molecular appearance are in good agreement (Figure 1f).

Furthermore, we systematically investigated the DOS of the CuCRs using DFT calculations. Figure 3a displays a series of spin-polarized DOS of free-standing *N*-CuCRs with different widths. Intriguingly, the asymmetric DOS for spin-up and spin-down components indicates a spin polarization of the CuCRs, although the incorporated Cu atoms in the chains are not magnetically active, which is similar to our previous studies.[24] More interestingly, the CuCRs exhibit a width-dependent band gap modulation. The calculated band gap decreases from 4.02 to 2.38 eV with an increasing width (*N*) from 1 to 5 (Figure 3a). The corresponding projected DOS (PDOS) on the C_{sp}, Cu_{sp}, and Cu_d orbitals of CuCRs was also calculated to show contributions of different orbitals to the band gap narrowing, where the C_{sp} and Cu_d orbitals contribute to the highest occupied molecular orbitals and the C_{sp} and Cu_{sp} orbitals contribute to the lowest unoccupied molecular orbital of CuCRs (Figure S2). In a quasi-one-dimensional system, the band gap reduction as a function of ribbon width was reported in free-standing armchair graphene nanoribbons (AGNRs), owing to the reduced electron−electron interaction and weaker quantum confinement effect. In other words, the wider AGNRs are easier for electrons to redistribute and respond to the presence of the external field.[28−30] Unlike AGNRs, the CuCRs are formed by the self-assembly of individual Cu-carbyne chains instead of covalent bonding, and the band gap narrowing is also significant even with the interchain spacing up to ~3.5 Å (Figure S3).

To understand the width-dependent band gap reduction, as the next step, electron density difference (EDD) and interaction region indicator (IRI) analysis on CuCRs were further performed to investigate the interchain interactions, which may have an influence on the band gap. Figure 3c,d shows the EDD color-filled map and isosurface map of free-standing 3-CuCR as an example. From the EDD maps, electron depletion (blue isosurfaces) occurs between C≡C bonds in the adjacent Cu-carbyne chains. In contrast, the electron accumulation (yellow isosurfaces) can be clearly identified between the Cu atoms in the adjacent Cu-carbyne chains. The charge redistribution of CuCRs suggests that the interchain interaction is dominated by the interaction between Cu atom sites.

To illustrate the nature of interchain interactions of CuCRs, we used a finite hydrogen-terminated 3-CuCR as a model system in IRI and IRI-π analyses. IRI is a new real-space function that can clearly reveal both chemical bonds and weak interactions in chemical systems.[31] As illustrated in the IRI isosurface and color-filled maps (Figure 4a,b), both covalent bond and weak interaction regions are nicely revealed by the blue and green isosurfaces, respectively, according to the standard coloring method shown in Figure S4 (see more details in the Supporting Information). It thus demonstrates that CuCRs are stabilized by weak interactions between the Cu-carbyne chains. Notably, the 3-CuCR exhibits wider weak interaction regions between the Cu atoms than those between

https://doi.org/10.1021/jacs.2c12292
J. Am. Chem. Soc. 2023, 145, 6203−6209

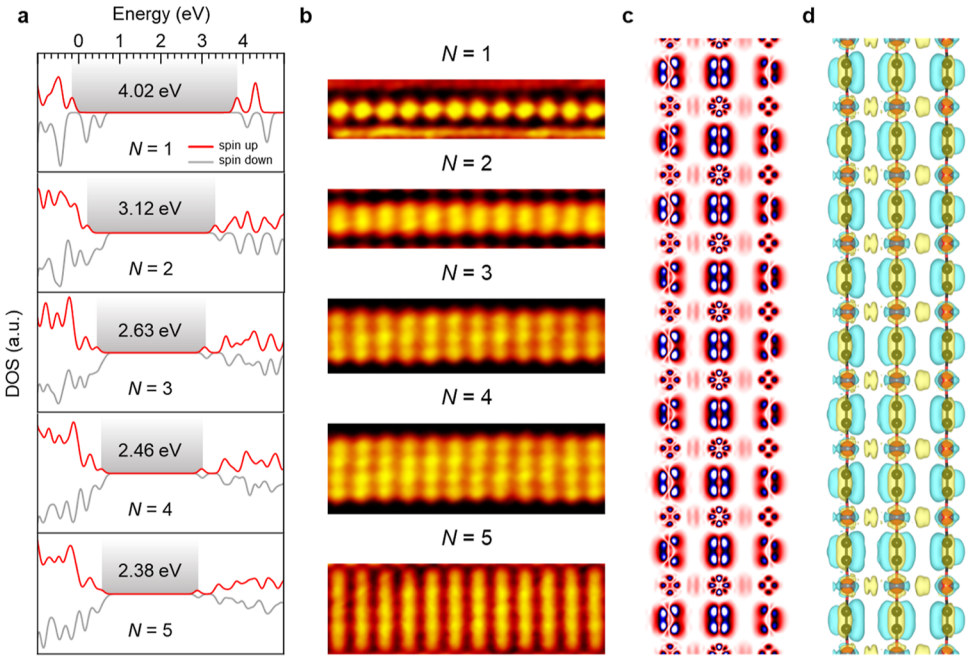

Figure 3. DFT calculated electronic properties of CuCRs with different widths. (a) Spin-polarized DOS and (b) corresponding STM images of *N*-CuCRs with different widths (N = 1, 2, 3, 4, and 5). Red and gray lines represent the spin-up and spin-down contributions, respectively. (c) EDD color-filled map and (d) isosurface map of 3-CuCR. Color-filled map is plotted on the ribbon plane. Yellow and blue isosurfaces represent the accumulation and depletion of electrons, respectively. Gray and red balls represent C and Cu atoms, respectively. Scanning conditions: V_t = −743 mV; I_t = 1.26 nA.

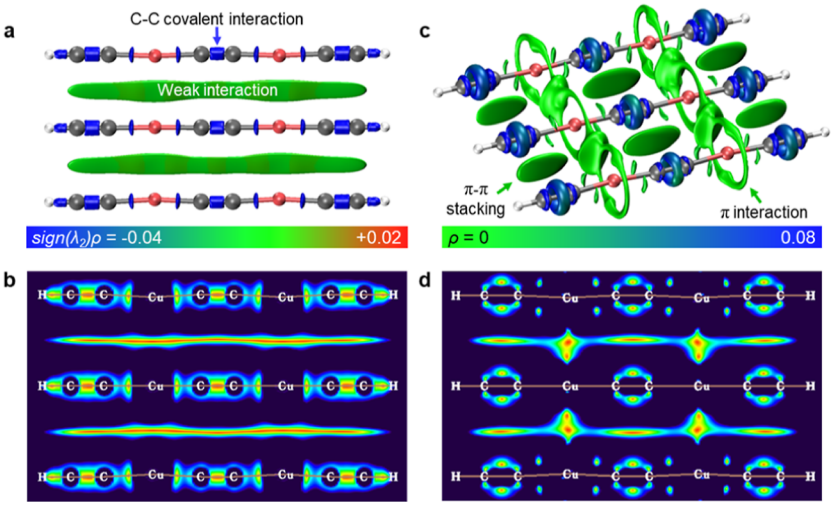

Figure 4. IRI maps of finite 3-CuCR. (a) IRI isosurface and (b) color-filled maps of finite 3-CuCR showing the weak interactions between neighboring Cu-carbyne chains. Blue and green isosurfaces represent the covalent interactions and weak interactions, respectively. (c) IRI-π isosurface and (d) color-filled maps of finite 3-CuCR showing the π interactions between Cu-carbyne chains. Color-filled maps are plotted on the ribbon plane. Gray, red, and white balls represent C, Cu, and H atoms, respectively. The scales of color bars are given in a.u.

carbon atoms, which is consistent with the EDD results. The isosurface and color-filled maps of the IRI function for the π molecular orbitals of 3-CuCR, referred to as IRI-π, are shown in Figure 4c,d to further reveal the interchain interactions. For each Cu-carbyne chain in 3-CuCR, the C≡C bonds exhibit torus-shaped IRI-π isosurfaces, maintaining the intrinsic double π (π^{in} and π^{out}) interaction features.[31,32] Besides, the weak single π interactions exist for C−Cu−C bonds, where the torus-shaped IRI-π isosurfaces near Cu atoms may arise from the $3d_{xz}/d_{yz}$ orbital, which initially exists in the individual Cu-carbyne chain[33] (see Figure S5). In the cross-chain regions, the IRI-π isosurfaces between the C≡C bonds are localized in the middle of the adjacent Cu-carbyne chains, indicating a weak face-to-face π−π stacking interaction, similar to the aromatic−aromatic interaction with sandwich configuration, which maximizes the overlap of π systems.[34,35] Significantly, the IRI-π isosurfaces around Cu atoms are broader and merge together in the middle of the chains, providing the intuitive evidence that the attractive force-driven orbital overlaps between Cu atoms across the chain, which is also consistent with the electron accumulation near the Cu atoms and electron depletion between C≡C bonds in EDD calculation. The color-filled IRI-π map can give the same conclusion from a complementary perspective. Given all this, it can be inferred

https://doi.org/10.1021/jacs.2c12292
J. Am. Chem. Soc. 2023, 145, 6203−6209

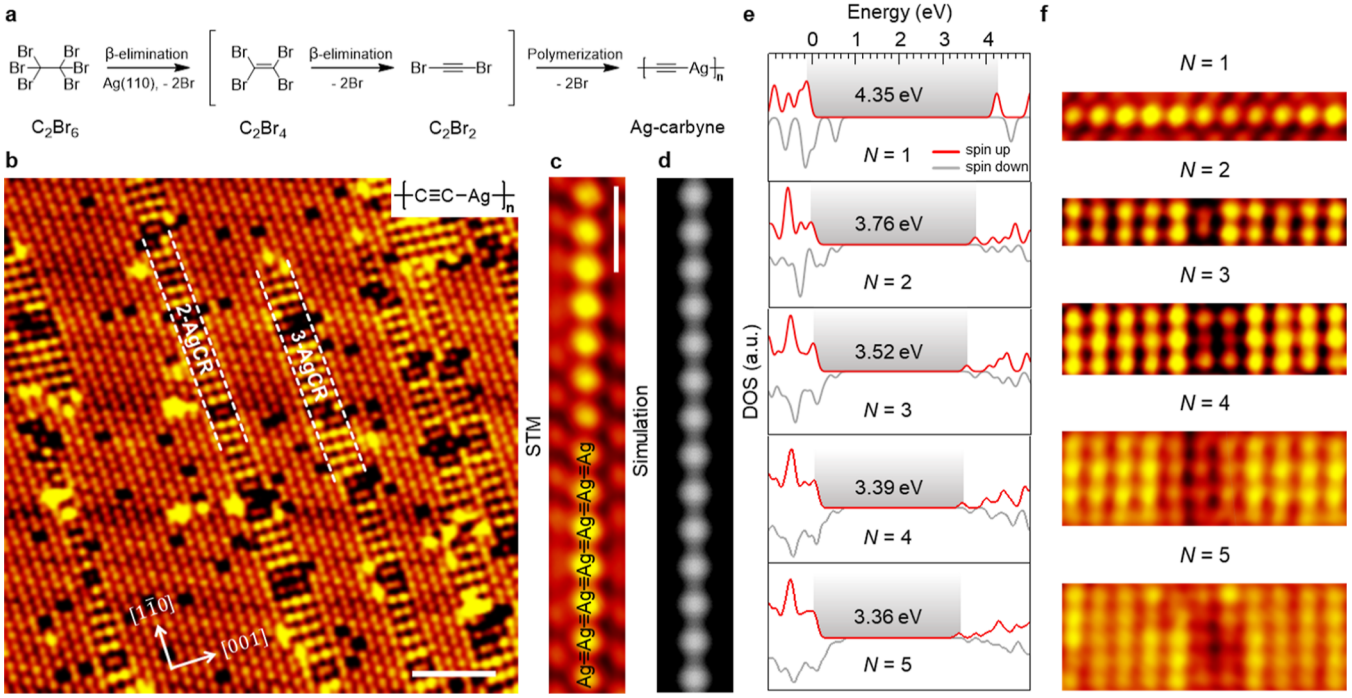

Figure 5. Bottom-up synthesis of AgCRs via sequential β-elimination reactions on Ag(110). (a) Schematic illustration of the bottom-up synthesis of Ag-carbyne via sequential β-elimination reactions from the C_2Br_6 precursor. (b) STM image showing the AgCRs obtained by depositing C_2Br_6 molecules on Ag(110) held at 300 K. Scale bar: 3 nm. (c) STM image and (d) simulated STM image of a single Ag-carbyne chain. Scale bars: 1 nm. (e) Spin-polarized DOS and (f) corresponding STM images of *N*-AgCRs with different widths (N = 1, 2, 3, 4, and 5). Red and gray lines represent the spin-up and spin-down contributions, respectively. Scanning conditions: V_t = −743 mV; I_t = 1.26 nA.

that the balance of the face-to-face $\pi-\pi$ stacking between C≡C bonds and the orbital overlap between Cu atoms stabilize the CuCR structure; as a result, the electrons are likely to delocalize across the CuCRs over the Cu atoms, which could be mainly responsible for the reduction of the band gap in wider CuCRs.[36,37]

To demonstrate the generality of elimination reactions and also introduce other transition-metal atoms in MCRs, we furthermore designed the C_2Br_6 precursor to synthesize AgCRs via sequential β-elimination reactions catalyzed by the Ag(110) surface (Figure 5). As expected, AgCRs were obtained from C_2Br_6 during an analogous, thermally induced elimination−polymerization procedure (Figure 5a), and the structural characterization is shown in Figure 5b. Based on the theoretical calculations (Figure S6), further STM simulation perfectly reproduces the morphology and periodicity of the acetylenic Ag-carbyne chain (Figure 5c,d). In addition, DFT calculated energetically most favorable reaction pathways demonstrate that sequential β-elimination reactions took place, leading to the formation of Ag-carbyne chains (see more details in Supporting Information Figure S7). AgCRs with different widths were also observed and analyzed by DFT-calculated spin-polarized DOS, indicating the analogous phenomena of band gap reduction (Figure 5e,f). Therefore, we have demonstrated the versatility of on-surface elimination reactions as an efficient way to synthesize different types of MCRs, and the width modification can serve as a generic useful strategy for engineering the band gap of MCRs.

CONCLUSIONS

We have successfully demonstrated the bottom-up synthesis of CuCRs and AgCRs via surface-catalyzed α- and β-elimination reactions, where metalated carbynes were packed in a metal-to-metal manner. The high-resolution capability of STM to resolve the morphology, in combination with extensive DFT calculations, provides valuable details on the growth pathway and electronic structure of MCRs. The electron delocalization across Cu-carbyne chains via d orbital overlap of the Cu atoms illuminates the band gap reduction in wider CuCRs, which was demonstrated by the IRI and IRI-π based on the wave function analysis. More importantly, by introducing on-surface elimination reactions, our study not only provides an efficient strategy for in situ fabrication of carbyne-like nanostructures such as MCRs but also complements the on-surface synthetic routes for broad carbon-rich nanomaterials. The band structure engineering strategy of MCRs based on the ribbon width may open up more opportunities for further exploration of semiconducting materials and molecular electronic devices.

EXPERIMENTAL AND THEORETICAL METHODS

Experimental Section. A variable-temperature "Aarhus-type" STM[38,39] was used for carrying out all the STM experiments including sample preparation, molecular evaporation, and characterization under ultrahigh vacuum conditions (with a base pressure below 3 × 10^{-10} mbar). The Cu(110) and Ag(110) single crystals were cleaned by repeated cycles of 1.5 keV argon ion sputtering followed by annealing at 800 K for 15 min. The CBr_4 and C_2Br_6 molecules were thoroughly degassed and then sublimated from quartz crucibles of molecular evaporators (with a typical sublimation temperature of 300 K) onto Cu(110) and Ag(110) held at 300 K. STM images were recorded in a constant-current mode, using an electrochemically etched tungsten tip. All the STM images were recorded at ∼100 K.

Theoretical Calculations. The spin-polarized DOS, PDOS, and elimination reaction pathway calculations were performed in the framework of DFT by using the Vienna ab initio simulation package (VASP).[40,41] The projector-augmented wave method[42,43] was used to describe the interaction between ions and electrons, and the Perdew−

https://doi.org/10.1021/jacs.2c12292
J. Am. Chem. Soc. 2023, 145, 6203−6209

Burke−Ernzerhof generalized gradient approximation exchange−correlation functional was employed.[44] The dispersion-corrected DFT-D3 method[45] was used to consider the van der Waals interactions. For the elimination reaction calculations, we used a $p(4 \times 6)$ surface unit cell of Cu(110) and Ag(110) with a $2 \times 2 \times 1$ gamma centered Monkhorst−Pack k-point grid. The kinetic energy cut-off was set to 400 eV. Transition states were searched by applying the climbing image nudged elastic band[46] and Dimer methods,[47] and all local minima and saddle points were optimized until the forces on all unconstrained atoms were ≤0.03 eV/Å. The IRI and IRI-π maps were calculated with B3LYP/6-31G** (Gaussian 09)[48] combined with Multiwfn 3.8.[49] The Tersoff−Hamann method[50] was used to obtain the simulated STM image.

■ ASSOCIATED CONTENT

Supporting Information

The Supporting Information is available free of charge at https://pubs.acs.org/doi/10.1021/jacs.2c12292.

Detailed descriptions of experimental and theoretical procedures and additional STM and DFT calculation results (PDF)

■ AUTHOR INFORMATION

Corresponding Author

Wei Xu − *Interdisciplinary Materials Research Center, School of Materials Science and Engineering, Tongji University, Shanghai 201804, People's Republic of China;* orcid.org/0000-0003-0216-794X; Email: xuwei@tongji.edu.cn

Authors

Wenze Gao − *Interdisciplinary Materials Research Center, School of Materials Science and Engineering, Tongji University, Shanghai 201804, People's Republic of China*

Liangliang Cai − *Interdisciplinary Materials Research Center, School of Materials Science and Engineering, Tongji University, Shanghai 201804, People's Republic of China; Department of Physics, National University of Singapore, Singapore 117551, Singapore*

Faming Kang − *Interdisciplinary Materials Research Center, School of Materials Science and Engineering, Tongji University, Shanghai 201804, People's Republic of China*

Lina Shang − *Interdisciplinary Materials Research Center, School of Materials Science and Engineering, Tongji University, Shanghai 201804, People's Republic of China*

Mali Zhao − *Interdisciplinary Materials Research Center, School of Materials Science and Engineering, Tongji University, Shanghai 201804, People's Republic of China*

Chi Zhang − *Interdisciplinary Materials Research Center, School of Materials Science and Engineering, Tongji University, Shanghai 201804, People's Republic of China*

Complete contact information is available at: https://pubs.acs.org/10.1021/jacs.2c12292

Author Contributions

[§]W.G. and L.C. contributed equally to this work.

Notes

The authors declare no competing financial interest.

■ ACKNOWLEDGMENTS

The authors acknowledge the financial support from the National Natural Science Foundation of China (22125203 and 21790351).

■ REFERENCES

(1) Kroto, H. W.; Heath, J. R.; O'Brien, S. C.; Curl, R. F.; Smalley, R. E. C_{60}: Buckminsterfullerene. *Nature* **1985**, *318*, 162−163.

(2) Iijima, S.; Ichihashi, T. Single-Shell Carbon Nanotubes of 1-nm Diameter. *Nature* **1993**, *363*, 603−605.

(3) Novoselov, K. S.; Geim, A. K.; Morozov, S. V.; Jiang, D.; Zhang, Y.; Dubonos, S. V.; Grigorieva, I. V.; Firsov, A. A. Electric Field Effect in Atomically Thin Carbon Films. *Science* **2004**, *306*, 666−669.

(4) Liu, M.; Artyukhov, V. I.; Lee, H.; Xu, F.; Yakobson, B. I. Carbyne from First Principles: Chain of C Atoms, a Nanorod or a Nanorope. *ACS Nano* **2013**, *7*, 10075−10082.

(5) Chalifoux, W. A.; Tykwinski, R. R. Synthesis of Polyynes to Model the sp-Carbon Allotrope Carbyne. *Nat. Chem.* **2010**, *2*, 967−971.

(6) Shi, L.; Rohringer, P.; Suenaga, K.; Niimi, Y.; Kotakoski, J.; Meyer, J. C.; Peterlik, H.; Wanko, M.; Cahangirov, S.; Rubio, A.; Lapin, Z. J.; Novotny, L.; Ayala, P.; Pichler, T. Confined Linear Carbon Chains as a Route to Bulk Carbyne. *Nat. Mater.* **2016**, *15*, 634−639.

(7) Lagow, R. J.; Kampa, J. J.; Wei, H.; Battle, S. L.; Genge, J. W.; Laude, D. A.; Harper, C. J.; Bau, R.; Stevens, R. C.; Haw, J. F.; Munson, E. Synthesis of Linear Acetylenic Carbon: The "sp" Carbon Allotrope. *Science* **1995**, *267*, 362−367.

(8) Homann, K. H. Fullerenes and Soot Formation-New Pathways to Large Particles in Flames. *Angew. Chem., Int. Ed.* **1998**, *37*, 2434−2451.

(9) Ho, C. L.; Yu, Z. Q.; Wong, W. Y. Multifunctional Polymetallaynes: Properties, Functions and Applications. *Chem. Soc. Rev.* **2016**, *45*, 5264−5295.

(10) Santhini, V. M.; Wäckerlin, C.; Cahlík, A.; Ondráček, M.; Pascal, S.; Matěj, A.; Stetsovych, O.; Mutombo, P.; Lazar, P.; Siri, O.; Jelínek, P. 1D Coordination π-d Conjugated Polymers with Distinct Structures Defined by the Choice of the Transition Metal: Towards a New Class of Antiaromatic Macrocycles. *Angew. Chem., Int. Ed.* **2021**, *60*, 439−445.

(11) Hanhart, W.; Ingold, C. K. CXXXIX.—the Nature of the Alternating Effect in Carbon Chains. Part XVIII. Mechanism of Exhaustive Methylation and its Relation to Anomalous Hydrolysis. *J. Chem. Soc.* **1927**, *0*, 997−1020.

(12) Sicher, J.; Havel, M.; Svoboda, M. Preferred Overall Syn-Elimination in Metal Promoted Cycloalkene Formation From Vicinal Dibromides. *Tetrahedron Lett.* **1968**, *9*, 4269−4272.

(13) Garst, J. F.; Pacifici, J. A.; Singleton, V. D.; Ezzel, M. F.; Morris, J. I. Dehalogenations of 2,3-Dihalobutanes by Alkali Naphthalenes. Cidnp [Chemically Induced Dynamic Nuclear Polarization] and Stereochemical Study. *J. Am. Chem. Soc.* **1975**, *97*, 5242−5249.

(14) Martin, J. D.; Perez, C.; Ravelo, J. L. Stereocontrolled Syntheses of (E)- And (Z)-.Gamma.-Bisabolene 8,9-Epoxide. *J. Am. Chem. Soc.* **1985**, *107*, 516−518.

(15) Krespan, C. G.; Harder, R. J.; Drysdale, J. J. Bis-(Polyfluoroalkyl)-Acetylenes. I. Synthesis of Bis-(Polyfluoroalkyl)-Acetylenes. *J. Am. Chem. Soc.* **1961**, *83*, 3424−3427.

(16) Köbrich, G. Eliminations From Olefins. *Angew. Chem., Int. Ed.* **1965**, *4*, 49−68.

(17) Krebs, A.; Swienty-Busch, J. 5.1-Eliminations to Form Alkenes, Allenes and Alkynes and Related Reactions. *Comprehensive Organic Synthesis*; Elsevier, 1991; pp 949−973.

(18) Irwin, M. J.; Jia, G.; Payne, N. C.; Puddephatt, R. J. Rigid-Rod Polymers and Model Compounds with Gold(I) Centers Bridged by Diisocyanides and Diacetylides. *Organometallics* **1996**, *15*, 51−57.

(19) Kaiser, K.; Scriven, L. M.; Schulz, F.; Gawel, P.; Gross, L.; Anderson, H. L. An sp-Hybridized Molecular Carbon Allotrope, Cyclo[18]Carbon. *Science* **2019**, *365*, 1299−1301.

(20) Sun, Q.; Cai, L.; Wang, S.; Widmer, R.; Ju, H.; Zhu, J.; Li, L.; He, Y.; Ruffieux, P.; Fasel, R.; Xu, W. Bottom-Up Synthesis of Metalated Carbyne. *J. Am. Chem. Soc.* **2016**, *138*, 1106−1109.

(21) Sun, Q.; Yu, X.; Bao, M.; Liu, M.; Pan, J.; Zha, Z.; Cai, L.; Ma, H.; Yuan, C.; Qiu, X.; Xu, W. Direct Formation of C−C Triple-Bonded Structural Motifs by On-Surface Dehalogenative Homocou-

plings of Tribromomethyl-Substituted Arenes. *Angew. Chem., Int. Ed.* **2018**, *57*, 4035−4038.
(22) Yu, X.; Li, X.; Lin, H.; Liu, M.; Cai, L.; Qiu, X.; Yang, D.; Fan, X.; Qiu, X.; Xu, W. Bond-Scission-Induced Structural Transformation from Cumulene to Diyne Moiety and Formation of Semiconducting Organometallic Polyyne. *J. Am. Chem. Soc.* **2020**, *142*, 8085−8089.
(23) Gao, W.; Kang, F.; Qiu, X.; Yi, Z.; Shang, L.; Liu, M.; Qiu, X.; Luo, Y.; Xu, W. On-Surface Debromination of C_6Br_6: C_6 Ring Versus C_6 Chain. *ACS Nano* **2022**, *16*, 6578−6584.
(24) Yu, X.; Sun, Q.; Liu, M.; Du, W.; Liu, Y.; Cai, L.; Zha, Z.; Pan, J.; Kang, F.; Gao, W.; Yang, D.; Qiu, X.; Xu, W. Lattice-Directed Selective Synthesis of Acetylenic and Diacetylenic Organometallic Polyynes. *Chem. Mat.* **2022**, *34*, 1770−1777.
(25) Wang, W.; Shi, X.; Wang, S.; Van Hove, M. A.; Lin, N. Single-Molecule Resolution of an Organometallic Intermediate in a Surface-Supported Ullmann Coupling Reaction. *J. Am. Chem. Soc.* **2011**, *133*, 13264−13267.
(26) Sun, Q.; Cai, L.; Ma, H.; Yuan, C.; Xu, W. Dehalogenative Homocoupling of Terminal Alkynyl Bromides on Au(111): Incorporation of Acetylenic Scaffolding into Surface Nanostructures. *ACS Nano* **2016**, *10*, 7023−7030.
(27) Kong, Q.; Wulff, M.; Lee, J. H.; Bratos, S.; Ihee, H. Photochemical Reaction Pathways of Carbon Tetrabromide in Solution Probed by Picosecond X-Ray Diffraction. *J. Am. Chem. Soc.* **2007**, *129*, 13584−13591.
(28) Deniz, O.; Sánchez-Sánchez, C.; Dumslaff, T.; Feng, X.; Narita, A.; Müllen, K.; Kharche, N.; Meunier, V.; Fasel, R.; Ruffieux, P. Revealing the Electronic Structure of Silicon Intercalated Armchair Graphene Nanoribbons by Scanning Tunneling Spectroscopy. *Nano Lett.* **2017**, *17*, 2197−2203.
(29) Merino-Díez, N.; Garcia-Lekue, A.; Carbonell-Sanromà, E.; Li, J.; Corso, M.; Colazzo, L.; Sedona, F.; Sánchez-Portal, D.; Pascual, J. I.; de Oteyza, D. G. Width-Dependent Band Gap in Armchair Graphene Nanoribbons Reveals Fermi Level Pinning on Au(111). *ACS Nano* **2017**, *11*, 11661−11668.
(30) Yang, L.; Park, C. H.; Son, Y. W.; Cohen, M. L.; Louie, S. G. Quasiparticle Energies and Band Gaps in Graphene Nanoribbons. *Phys. Rev. Lett.* **2007**, *99*, 186801.
(31) Lu, T.; Chen, Q. Interaction Region Indicator: A Simple Real Space Function Clearly Revealing Both Chemical Bonds and Weak Interactions**. *Chem. Methods* **2021**, *1*, 231−239.
(32) Wang, X.; Liu, Z.; Yan, X.; Lu, T.; Zheng, W.; Xiong, W. Bonding Character, Electron Delocalization, and Aromaticity of Cyclo[18]Carbon (C_{18}) Precursors, C_{18}-$(Co)_n$ (n = 6, 4, and 2): Focusing on the Effect of Carbonyl (-Co) Groups**. *Chem.—Eur. J.* **2022**, *28*, No. e202103815.
(33) Tu, X.; Wang, H.; Shen, Z.; Wang, Y.; Sanvito, S.; Hou, S. Cu-Metalated Carbyne Acting as a Promising Molecular Wire. *J. Chem. Phys.* **2016**, *145*, 244702.
(34) Chen, T.; Li, M.; Liu, J. π-π Stacking Interaction: A Nondestructive and Facile Means in Material Engineering for Bioapplications. *Cryst. Growth Des.* **2018**, *18*, 2765−2783.
(35) Hunter, C. A.; Sanders, J. K. M. The Nature of π-π Interactions. *J. Am. Chem. Soc.* **1990**, *112*, 5525−5534.
(36) Steiner, C.; Gebhardt, J.; Ammon, M.; Yang, Z.; Heidenreich, A.; Hammer, N.; Görling, A.; Kivala, M.; Maier, S. Hierarchical On-Surface Synthesis and Electronic Structure of Carbonyl-Functionalized One- and Two-Dimensional Covalent Nanoarchitectures. *Nat. Commun.* **2017**, *8*, 14765.
(37) Gutzler, R.; Perepichka, D. F. π-Electron Conjugation in Two Dimensions. *J. Am. Chem. Soc.* **2013**, *135*, 16585−16594.
(38) Laegsgaard, E.; Österlund, L.; Thostrup, P.; Rasmussen, P. B.; Stensgaard, I.; Besenbacher, F. A High-Pressure Scanning Tunneling Microscope. *Rev. Sci. Instrum.* **2001**, *72*, 3537−3542.
(39) Besenbacher, F. Scanning Tunnelling Microscopy Studies of Metal Surfaces. *Rep. Prog. Phys.* **1996**, *59*, 1737−1802.
(40) Kresse, G.; Hafner, J. Ab Initio Molecular Dynamics for Open-Shell Transition Metals. *Phys. Rev. B: Condens. Matter Mater. Phys.* **1993**, *48*, 13115−13118.
(41) Kresse, G.; Furthmüller, J. Efficient Iterative Schemes for Ab Initio Total-Energy Calculations Using a Plane-Wave Basis Set. *Phys. Rev. B: Condens. Matter Mater. Phys.* **1996**, *54*, 11169−11186.
(42) Blöchl, P. E. Projector Augmented-Wave Method. *Phys. Rev. B: Condens. Matter Mater. Phys.* **1994**, *50*, 17953−17979.
(43) Kresse, G.; Joubert, D. From Ultrasoft Pseudopotentials to the Projector Augmented-Wave Method. *Phys. Rev. B: Condens. Matter Mater. Phys.* **1999**, *59*, 1758−1775.
(44) Perdew, J. P.; Burke, K.; Ernzerhof, M. Generalized Gradient Approximation Made Simple. *Phys. Rev. Lett.* **1996**, *77*, 3865−3868.
(45) Grimme, S.; Antony, J.; Ehrlich, S.; Krieg, H. A Consistent and Accurate Ab Initio Parametrization of Density Functional Dispersion Correction (Dft-D) for the 94 Elements H-Pu. *J. Chem. Phys.* **2010**, *132*, 154104.
(46) Henkelman, G.; Uberuaga, B. P.; Jónsson, H. A Climbing Image Nudged Elastic Band Method for Finding Saddle Points and Minimum Energy Paths. *J. Chem. Phys.* **2000**, *113*, 9901−9904.
(47) Kästner, J.; Sherwood, P. Superlinearly Converging Dimer Method for Transition State Search. *J. Chem. Phys.* **2008**, *128*, 014106.
(48) Frisch, M. J.; Trucks, G. W.; Schlegel, H. B.; Scuseria, G. E.; Robb, M. A.; Cheeseman, J. R.; Scalmani, G.; Barone, V.; Petersson, G. A.; Nakatsuji, H.; Li, X.; Caricato, M.; Marenich, A. V.; Bloino, J.; Janesko, B. G.; Gomperts, R.; Mennucci, B.; Hratchian, H. P.; Ortiz, J. V.; Izmaylov, A. F.; et al. *Gaussian 09*. Revision A.02; Gaussian, Inc.: Wallingford, CT, 2016.
(49) Lu, T.; Chen, F. Multiwfn: A Multifunctional Wavefunction Analyzer. *J. Comput. Chem.* **2012**, *33*, 580−592.
(50) Tersoff, J.; Hamann, D. Theory of the Scanning Tunneling Microscope. *Phys. Rev. B: Condens. Matter Mater. Phys.* **1985**, *31*, 805−813.

https://doi.org/10.1021/jacs.2c12292
J. Am. Chem. Soc. 2023, 145, 6203−6209